Published in final edited form as:

Nature. 2016 November 03; 539(7627): 54–58. doi:10.1038/nature20099.

Break-induced telomere synthesis underlies alternative telomere maintenance

Robert L. Dilley[1], **Priyanka Verma**[1], **Nam Woo Cho**[1], **Harrison D. Winters**[1], **Anne R. Wondisford**[1], and **Roger A. Greenberg**[1,2]

[1]Department of Cancer Biology, Abramson Family Cancer Research Institute, Basser Research Center for BRCA, Perelman School of Medicine, University of Pennsylvania, 421 Curie Boulevard, Philadelphia, Pennsylvania 19104, USA

[2]Department of Pathology, Abramson Family Cancer Research Institute, Basser Research Center for BRCA, Perelman School of Medicine, University of Pennsylvania, 421 Curie Boulevard, Philadelphia, Pennsylvania 19104, USA

Abstract

Homology-directed DNA repair is essential for genome maintenance through templated DNA synthesis. Alternative lengthening of telomeres (ALT) necessitates homology-directed DNA repair to maintain telomeres in about 10–15% of human cancers. How DNA damage induces assembly and execution of a DNA replication complex (break-induced replisome) at telomeres or elsewhere in the mammalian genome is poorly understood. Here we define break-induced telomere synthesis and demonstrate that it utilizes a specialized replisome, which underlies ALT telomere maintenance. DNA double-strand breaks enact nascent telomere synthesis by long-tract unidirectional replication. Proliferating cell nuclear antigen (PCNA) loading by replication factor C (RFC) acts as the initial sensor of telomere damage to establish predominance of DNA polymerase δ (Pol δ) through its POLD3 subunit. Break-induced telomere synthesis requires the RFC–PCNA–Pol δ axis, but is independent of other canonical replisome components, ATM and ATR, or the homologous recombination protein Rad51. Thus, the inception of telomere damage recognition by the break-induced replisome orchestrates homology-directed telomere maintenance.

Tremendous progress has been made in identifying the events responsible for recognizing and repairing DNA double-strand breaks (DSBs)[1]. A complex aspect of this response is homology-directed DNA repair (HDR), which can involve numerous possibilities to capture homologous regions of the genome to use for templated DNA synthesis and repair. The

Correspondence and requests for materials should be addressed to: R.A.G. (rogergr@mail.med.upenn.edu).

Online Content Methods, along with any additional Extended Data display items and Source Data, are available in the online version of the paper; references unique to these sections appear only in the online paper.

Supplementary Information is available in the online version of the paper.

Author Contributions R.L.D., P.V., N.W.C., and R.A.G. designed the study. R.L.D. performed most of the experiments, with assistance from H.D.W. and A.R.W. P.V. conducted SMARD experiments. N.W.C. conducted ATR and Hop2 experiments. R.L.D., P.V., and R.A.G. wrote the manuscript.

The authors declare no competing financial interests. Readers are welcome to comment on the online version of the paper.

detailed order of molecular events that ensues after the initial sensing of DSBs to allow the execution of homology-directed synthesis remains enigmatic. Specifically, how the DNA damage response coordinates productive interactions between DNA replication complexes to perform break-induced DNA synthesis has not been extensively demonstrated in mammalian cells. ALT is a clinically relevant example of a DNA repair pathway that requires homology-directed synthesis to maintain telomeres in ~10–15% of human cancers[2,3]. Additionally, such synthesis could represent an attractive therapeutic target against cancers, especially if it proves to be different from canonical S-phase replication.

Telomere breaks stimulate long-tract synthesis

To study homology-directed synthesis at ALT telomeres, we developed a bromodeoxyuridine (BrdU) pulldown approach to isolate and quantify nascent telomeres synthesized following telomere-targeted DSBs generated by the fusion of the Shelterin component TRF1to the FokI endonuclease (Fig. 1a). Using stable ALT-positive U2OS cell lines expressing TRF1–FokI under tetracycline-control, a 2-h damage induction with wild-type TRF1–FokI, but not the FokI(D450A) nuclease-null mutant, resulted in a ~10-fold increase in nascent telomere synthesis in asynchronous and G2-enriched cells (Fig. 1b, c and Extended Data Fig. 1a–g). Concurrent synthesis of nascent C- and G-rich telomere strands was evident from 1 h post-induction and became maximal at ~2h (Fig. 1d). Nascent Alu repeat DNA was not increased by TRF1–FokI expression, demonstrating the specificity of break-induced telomere synthesis (Fig. 1d).

To understand the nature of individual DNA synthesis events, we adapted the single-molecule analysis of replicated DNA (SMARD) technique for studying break-induced telomere synthesis[4,5]. After induction of TRF1–FokI, U2OS cells were sequentially incubated with iododeoxyuridine (IdU) and chlorodeoxyuridine (CIdU), genomic DNA was digested, and telomere fragments were isolated on the basis of size (Fig. 1e). The percentage of telomeres with IdU/CIdU incorporation increased with the duration of TRF1–FokI induction (Fig. 1f, g). Break-induced telomere synthesis proceeded in a unidirectional fashion, often to the end of the telomere fragment. Nascent telomere tracts ranged in length from 5 to 70 kilobases (kb), with a median value of 19.8 kb ($n = 46$) that matched the median length of the overall telomere fibres observed (20.1 kb; $n = 45$) (Fig. 1h). Furthermore, ~80% of nascent telomere fragments were completely labelled and ~98% of nascent fragments had label on at least one of the ends. Taken together, these data suggest that DSBs at ALT telomeres induce long-tract telomeric DNA synthesis.

As a complementary approach, BrdU immunofluorescence at telomeres provides a means to assess spontaneous synthesis of ALT telomeres. Cell lines that utilize ALT, but not telomerase, displayed elevated BrdU incorporation at telomeres in a pattern distinct from S-phase replication (Extended Data Fig. 2a, b, d), consistent with previous reports[6]. TRF1–FokI expression increased analogue incorporation at ALT telomeres in interphase and metaphase cells (Extended Data Fig. 2c, e), suggesting that telomere damage may be an initiating event for spontaneous ALT telomere synthesis[7].

Expanding on our observations, we generated a panel of TRF1–FokI inducible lines from cells that either utilize ALT (U2OS, VA13, SKNFI) or telomerase (HeLa 1.3, HeLa S3, 293T) for telomere maintenance. Notably, all lines showed evidence of break-induced telomere synthesis by BrdU pulldown upon induction with TRF1–FokI (Extended Data Fig. 3a–c). This holds true not only across telomere maintenance mechanism, but also regardless of ATRX status, overall telomere length differences, and cell type (Extended Data Fig. 3a). Notably, a recent study provided evidence that replication stress can activate ALT mechanisms in primary and telomerase-positive cells[8]. We propose that although any cell may have the capacity for break-induced telomere synthesis, ALT-positivity entails greater levels of telomere damage that promotes homology-directed DNA synthesis and telomere maintenance. Therefore, non S-phase telomere synthesis (Extended Data Fig. 2a, b, d) is apparent at baseline only in ALT cells.

Break-induced telomere synthesis by alternative HDR

Genetic studies in yeast demonstrated that break-induced replication is responsible for telomere recombination, which can proceed through Rad51-dependent and -independent mechanisms[9–15]. Rad51, together with the Hop2–Mnd1 heterodimer, localize to ALT-associated PML bodies (APBs) and facilitate long-range telomere movement and clustering in ALT cells[7,16,17]. Cells lacking Hop2 from CRISPR–Cas9-mediated excision showed reduced telomere clustering, APB formation, and telomere exchanges in ALT-positive VA13 cells (Extended Data Fig. 4a–f). ATR is a damage-sensing kinase that signals replication stress and is important for ALT telomere integrity and cell survival[18]. Disruption of ATR and Chk1 signalling by knockdown and small-molecule inhibitors reduced Hop2 recruitment to telomeres after TRF1–FokI induced damage, whereas ATM disruption had no effect (Fig. 2a). Similarly, ATR knockdown restricted telomere mobility after TRF1–FokI induction in U2OS cells (Fig. 2b), thus implicating ATR and Rad51–Hop2 as critical for ALT telomere mobility.

We next asked whether ATR and Rad51–Hop2 are required for break-induced telomere synthesis. Surprisingly, ATR, Rad51, and Hop2 were all dispensable for synthesis. Conversely, knockdown of each gene paradoxically increased levels of nascent telomeres, which held true over an 8-h time course (Fig. 2c, Extended Data Fig. 5a). Similarly, spontaneous ALT telomere synthesis did not require Rad51 (Extended Data Fig. 5e, i). To investigate the long-term consequences of depletion of this pathway, we examined the telomere length of VA13 *HOP2* CRISPR clones. All of the 6 clones lacked detectable Hop2 protein expression, with no telomere shortening observed at approximately population doubling (PD) 25 or longer time points (Extended Data Fig. 4g, h). Collectively, this provides evidence for Rad51-independent mechanisms of mammalian break-induced telomere synthesis and ALT telomere maintenance. Although ATR regulates damage signalling, telomere integrity, and survival in ALT cells, our data suggest it is not an essential component of the break-induced replisome at telomeres.

Break-induced telomere synthesis requires Pol δ

We next surveyed the replisome dependencies of break-induced telomere synthesis. Replicative DNA polymerases Pol δ, Pol ε, and Pol α-primase were previously implicated in yeast break-induced replication[12,19]. Pol δ, including the POLD3 and POLD4 accessory and POLD1 catalytic subunits, was required for break-induced telomere synthesis (Fig. 2d, e, Extended Data Fig. 5a, b, d). Unexpectedly, Pol δ was required for synthesis of both C- and G-rich telomere strands, whereas Pol ε and Pol α-primase were dispensable as was the MCM2-7 replicative helicase (Fig. 2d, f). Notably, depletion of POLD3 resulted in ~2.5-fold less incorporation of IdU/CIdU in telomere fibres after TRF1–FokI-induced breaks (Fig. 2g). POLD3 is also part of the Pol ζ complex involved in translesion synthesis[20–22]. However, the catalytic subunit of Pol ζ (REV3L) as well as the other translesion synthesis proteins Pol η (POLH) and REV1 were not needed for break-induced telomere synthesis (Fig. 2d, Extended Data Fig. 5c). Therefore, the major function of POLD3 in break-induced telomere synthesis is through Pol δ. Notably, the requirements for break-induced telomere synthesis using TRF1–FokI faithfully recapitulate the requirements for spontaneous ALT telomere synthesis. Specifically, non S-phase telomere synthesis in three ALT lines required POLD3/Pol δ, but occurred independently of Pol ε, Pol α, and Pol ζ (Extended Data Fig. 5f–i). Collectively, these data define a non-canonical replisome involved in ALT telomere synthesis.

RFC–PCNA is the initial sensor of telomere damage

Pol δ showed robust recruitment to TRF1–FokI damage sites in U2OS cells, whereas Pol ε, Pol α-primase, and MCM2-7 were present at much lower levels (Fig. 3a, Extended Data Fig. 6a, b). POLD3 facilitates interaction of the Pol δ complex with the PCNA clamp for processive synthesis and strand displacement[23]. Notably, Pol δ has higher affinity for PCNA than does Pol ε, and PCNA is known to function in repair processes outside S-phase[24,25]. Deletion of the PCNA-interacting peptide (PIP) box (Δ456–466) of POLD3 disrupted its recruitment to damage sites (Fig. 3b). Functionally, PCNA interaction with POLD3 facilitates recruitment of the whole Pol δ complex to damaged ALT telomeres (Extended Data Fig. 6c, d). The RFC1–5 clamp loading complex was required for PCNA–POLD3 telomere localization, whereas the alternative clamp loader subunit, Rad17 was dispensable (Fig. 3c). Furthermore, the entire axis consisting of RFC1–PCNA–POLD3 localized in an inducible fashion to ~90% of damaged ALT telomeres and was required for break-induced telomere synthesis (Fig. 3d, Extended Data Fig. 5h, 6e, f).

Both PCNA and POLD3 showed ~10-fold increases in telomere localization by 30 min after induction with TRF1–FokI (Fig. 3e). By contrast, Rad51 localization occurred more slowly and was maximal by 2 h after induction (Fig. 3e). Peak telomere synthesis coincided with an increase in DSB signalling (Figs 1d, 3e). Time-lapse imaging revealed that GFP–PCNA localized to TRF1–FokI damage sites soon after they became visible and before ALT telomere merging events (Fig. 3f, $n = 20$ cells). Consistent with PCNA loading being an early damage response, its localization was independent of proximal damage response factors ATR, ATM, MRE11, or homologous recombination proteins Rad51, Hop2, and BRCA2 (Fig. 3g). Importantly, RFC1, PCNA, and POLD3 spontaneously localized to ~2–

10% of telomeres specifically in ALT-positive cells, consistent with the presence of persistent damage at a subset of ALT telomeres[17] (Fig. 3h). These data reveal that PCNA loading is the initial damage sensor at ALT telomeres, thus establishing a platform to assemble the break-induced replisome.

POLD3 is critical for ALT telomere maintenance

Pol32, the yeast homologue of POLD3, is required for recombination dependent survivors of telomerase defiency[12]. Transient knockdown of POLD3 decreased spontaneous ALT telomere synthesis and single- telomere-exchange events by chromosome orientation fluorescence *in situ* hybridization (CO–FISH), but had no immediate effect on C-circles or telomere length (Extended Data Figs 5f–i, 7a, b). We investigated the consequences of prolonged POLD3 depletion on ALT telomere maintenance using CRISPR–Cas9 in U2OS cells. Although we were unable to generate surviving cells with complete loss of POLD3, we obtained 4 clones (c1–c4) with in-frame deletions and residual expression of POLD3 (Extended Data Fig. 7c–g). Notably, all 4 clones had reduced levels of the entire Pol δ complex (Fig. 4a, Extended Data Fig. 7g), consistent with a stabilizing role for POLD3 (ref. 26). Clones c1–c3 displayed accelerated telomere shortening at ~PD 25 compared to the empty guide control, whereas clone c4 had a more minor phenotype (Fig. 4b, Extended Data Fig. 7h, i). Telomere length in 5 clones with normal POLD3 expression (c5–c9) was unchanged at ~PD 25 (Extended Data Fig. 8a). The telomere shortening observed in clones c1–c3 is greater than expected for cells lacking a telomere maintenance mechanism, representing a loss of ~800–1200 bp of telomeric repeats per cell division. However, telomeres did not continue to shorten over time in these clones. This is consistent with accelerated shortening and stabilization observed in other ALT lines in which telomere maintenance mechanisms have been partially impaired[27]. Additional U2OS *POLD3* CRISPR clones from an independent guide RNA also displayed shortened telomeres compared to the parental line or clones derived from the same guide RNA that failed to exhibit reduced POLD3 expression, making it unlikely that the effects observed are due to clonal variation (Extended Data Fig. 8c). Collectively, analysis of the mean telomere length of the 31 clones from both of the guide RNAs revealed a significant decrease in clones with reduced POLD3 expression compared to those with normal POLD3 expression (Fig. 4c). In contrast, telomere length changes were not observed in 11 *POLD3* CRISPR clones from telomerase-positive HeLa 1.3 cells (Extended Data Fig. 8d–f), suggesting an increased requirement of POLD3 for processive telomere synthesis during ALT.

U2OS *POLD3* CRISPR clones accumulated increased numbers of telomere dysfunction-induced foci (TIFs) (Fig. 4d, Extended Data Fig. 7i). C-circles are another marker of telomere maintenance specific to ALT-dependent cells[28]. Clones c1–c3 had significantly decreased levels of C-circles that could be rescued by reconstituting wild-type POLD3, whereas clones c5–c9 did not display similar reductions (Fig. 4e, Extended Data Figs 7i–k, 8b). These data are consistent with a partial disruption of ALT activity and telomere maintenance in clones c1–c3 (Extended Data Fig. 7i). We propose that POLD3 is critical for the majority of nascent telomere synthesis during ALT and therefore underlies long-term telomere maintenance and ALT activity.

Discussion

Direct visualization of the dynamic process of ALT telomere recombination reveals that rapid RFC-mediated PCNA loading at damaged telomeres is the initial sensor of telomere damage, thus connecting DSB recognition with the assembly of a specialized replisome capable of executing break-induced telomere synthesis (Fig. 4f). On the other hand, Rad51 and Hop2 loading and long-range homology searches occur more slowly and are dispensable for the bulk of homology-directed DNA synthesis at telomeres (Fig. 4f). We postulate that PCNA can load at alternative structures with recessed 3′-ends and preferentially recruit Pol δ owing to its higher affinity for PCNA compared with that of Pol ε [24]. In contrast to yeast break-induced replication, Rad51 and Pol α-primase were not required for break-induced telomere synthesis. A repertoire of Rad51-independent mechanisms available to damaged telomeres, such as intra-telomere annealing or association with extra-chromosomal telomere repeats that are abundant in ALT cells may bypass the need for Rad51 and Pol α-mediated priming[3]. Persistent damage at ALT telomeres probably promotes Rad51 and other competing repair mechanisms with differing kinetics of homology-directed telomere synthesis[7,17] (Fig. 4f). We speculate that related processes are invoked at other vulnerable regions of the genome[29–33]. The unique characteristics that differentiate this mechanism from scheduled S-phase replication may facilitate a better understanding of how alternative repair mechanisms enable genome evolution and enhance cancer cell fitness.

METHODS

Data reporting

No statistical methods were used to predetermine sample size.

Cell culture

U2OS, HeLa 1.3, HeLa S3, DLD-1, and 293T cell lines were grown in DMEM (Thermo Fisher) with 10% calf serum and 1% penicillin/streptomycin. VA13, GM847, LM216T, and LM216J cell lines were grown in DMEM (Thermo Fisher) with 10% FBS and 1% penicillin/streptomycin. SKNFI cell line was grown in RPMI (Thermo Fisher) with 10% FBS and 1% penicillin/streptomycin. VA13 cell line refers to WI-38 VA-13 subline 2RA. LM216T/J are matched lines. Cell lines were obtained from ATCC and tested negative for Mycoplasma using the MycoAlert PLUS Mycoplasma Detection Kit (Lonza). The U2OS TRF1–FokI inducible cell line was authenticated by STR analysis (ATCC). Other lines were validated by ALT characteristics. None of the cell lines used is listed as commonly misidentified by the International Cell Line Authentication Committee (ICLAC).

ALT-positive lines used: U2OS, VA13, GM847, LM216J, SKNFI

ALT-negative lines used: HeLa 1.3 (long telomere), HeLa S3, DLD-1, LM216T, 293T

BrdU immunofluorescence

Cells were pulsed with 100 μM BrdU (Sigma) for 2 h before fixation. After permeabilization, cells were denatured with 500 U ml^{-1} DNaseI (Roche) in 1× reaction buffer (20 mM Tris-HCl (pH 8.4), 2 mM $MgCl_2$, 50 mM KCl in PBST) for 10–25 min at

37 °C in a humidified chamber. Coverslips were then washed and incubated with anti-BrdU antibody (BD) for 20 min at 37 °C followed by secondary antibody and telomere FISH. For metaphases, cells pulsed with BrdU were treated with 100 ng ml^{-1} colcemid for 90 min followed by 75 mM KCl for 30 min. Cells were fixed in 3:1 methanol:acetic acid, dropped onto slides, and allowed to dry overnight. Denaturation was performed with 2 N HCl for 30 min at room temperature followed by antibody incubations as described above.

BrdU pulldown dot blot

BrdU pulldown was adapted from a published protocol[34]. Cells were pulsed with 100 μM BrdU (Sigma) for 2 h before collection. Genomic DNA (gDNA) was isolated using phenol–chloroform extraction followed by resuspension in TE buffer. gDNA was then sheared into 100–300 bp fragments using a Covaris S220 sonicator. 1–4 μg sheared gDNA was denatured for 10 min at 95 °C and cooled in an ice-water bath. Denatured gDNA was incubated with 2 μg anti-IgG (Sigma) or anti-BrdU antibody (BD) diluted in immunoprecipitation buffer (0.0625% (v/v) Triton X-100 in PBS) rotating overnight at 4 °C. The next day, samples were incubated with 30 μl Protein G magnetic beads (Pierce) that had been pre-bound to a bridging antibody (Active Motif) for 1 h rotating at 4 °C. Beads were subsequently washed three times with immunoprecipitation buffer and once with TE buffer. Beads were then incubated twice in elution buffer (1% (w/v) SDS in TE) for 15 min at 65 °C. Pooled eluate was cleaned with ChIP DNA Clean & Concentrator kit (Zymo). Samples, along with 10% inputs, were diluted into 2× SSC buffer, treated at 95 °C for 5 min, and dot-blotted onto an Amersham Hybond-N^+ nylon membrane (GE). The membrane was then denatured in a 0.5 N NaOH 1.5 M NaCl solution, neutralized, and ultraviolet crosslinked. The membrane was hybridized with ^{32}P-labelled $(TTAGGG)_6$ oligonucleotides, unless otherwise noted, in PerfectHyb Plus Hybridization Buffer (Sigma) overnight at 37 °C. The next day, the membrane was washed twice in 2× SSC buffer, exposed onto a storage phosphor screen (GE Healthcare) and scanned using STORM 860 with ImageQuant (Molecular Dynamics). All quantifications were performed in Fiji and normalized to 10% input.

Telomere single-molecule analysis of replicated DNA (SMARD)

The SMARD assay was performed as previously described[4,5]. U2OS cells were induced with TRF1–FokI for 20 min or 2 h and were subsequently labelled by incubating with 30 μM IdU for 2 h, followed by 30 μM CIdU for the next 2 h. After pulsing, 10^6 labelled cells per condition were embedded in 1% agarose and lysed using detergents (100 mM EDTA, 0.2% sodium deoxycholate, 1% sodium lauryl sarcosine and 0.2 mg ml^{-1} Proteinase K). The plugs were then washed several times with TE, treated with 100 μM PMSF, and then washed again with TE buffer followed by incubation with 1× Cut-Smart buffer (NEB) for 30 min. The DNA in the plugs was then digested overnight at 37 °C using 50 U of both MboI and AluI (NEB) per plug. The digested plugs were then cast into a 0.7% low-melting point agarose gel and a distinct fragment running above 10 kb (containing telomeric DNA defined by Southern blotting) was excised, melted and stretched on slides coated with 3-aminopropoyltriethoxysilane (Sigma-Aldrich). After denaturation of the DNA strands using alkali buffer (0.1 M NaOH in 70% ethanol and 0.1% β-mercaptoethanol), the DNA was fixed using 0.5% glutaraldehyde and incubated overnight with biotin-OO-$(CCCTAA)_4$ locked nucleic acid (LNA) probe (Exiqon) at 37 °C. Telomere FISH probes were then

detected using the Alexa Fluor 405-conjugated streptavidin (Thermo-Fisher) followed by sequential incubation with the biotinylated anti-avidin antibody (Vector Laboratories) and additional Alexa 405-conjugated streptavidin. IdU and CldU were visualized using mouse anti-IdU (BD) and rat anti-CIdU (Serotec) monoclonal antibodies followed by Alexa Fluor 568-goat anti-mouse and Alexa Fluor 488-goat anti-rat secondary antibodies (Life Technologies). Images were acquired using the NIS-element software (Nikon) and a Nikon eclipse 80i microscope equipped with a 63× objective and a Cool Snap camera (MYO). For calculating the length of the telomeres and replication tracts, the line-scan function from Image J was used. For conversion of microns to kilobases, as 10 bp (equals one turn of the helix) has a linear length of 3.4 nm, 0.26 microns corresponded to 1 kb of DNA.

Plasmids, primers, siRNAs, and CRISPR sgRNAs

Death domain (DD)–Oestrogen receptor (ER)–mCherry–TRF1–FokI and Flag–TRF1–FokI constructs were cloned as previously described[7]. Doxycycline-inducible TRF1–FokI lines were generated using the Tet-On 3G system. Briefly, Flag–DD–ER–mCherry–TRF1–FokI was cloned into the pLenti CMV TRE3G Puro Dest vector, which was introduced into cells engineered to co-express the reverse tetracycline transactivator 3G (rtTA3G). N-terminal GFP-tagged proteins were generated by PCR amplification and ligation of cDNAs from the ProQuest HeLa cDNA Library (Invitrogen) into the pDEST53 (Invitrogen) mammalian expression vector. CRISPR lines were generated using a two-vector system (pLentiCas9-Blast and pLentiGuide-Puro). POLD3 reconstitution vector was generated by cloning POLD3 cDNA (RefSeq NM 006591.2) into the pOZ–N–Flag–HA retroviral vector followed by site- directed mutagenesis of siRNA binding sites. Sanger sequencing of *POLD3* CRISPR clones was performed on gDNA fragments cloned into a TOPO TA vector (Thermo Fisher).

Transient plasmid transfections were carried out with LipoD293 (Signagen), and siRNA transfections with Lipofectamine RNAiMax (Invitrogen) according to manufacturer's instructions. Analyses were performed 16 h after transfection of plasmids, and 72 h after siRNA transfection. All siRNAs were used at a final concentration of 20 nM.

The following primers were used for qRT–PCR:

POLD3 primer set 1: 5′-GAGTTCGTCACGGACCAAAAC-3′, 5′-GCCA GACACCAAGTAGGTAAC-3′;

POLD3 primer set 2: 5′-ACCAACAAGGAAACGAAAACAGA-3′, 5′-GG TTCCGTGACAGACACTGTA-3′;

The following siRNA sequences were used:

Control siRNA (siCtrl): QIAGEN AllStars Negative Control siRNA;

ATR siRNA (siATR): 5′-AACCUCCGUGAUGUUGCUUGAdTdT-3′;

ATM siRNA (siATM): 5′-GCGCCUGAUUCGAGAUCCUdTdT-3′;

RAD51 siRNA (siRAD51): #1, 5′-UGUAGCAUAUGCUCGAGCG-3′, #2, 5′-CCA GAUCUGUCAUACGCUA-3′;

HOP2 siRNA (siHOP2): #2, 5′-AAGAGAAGAUGUACGGCAA-3′, #3, 5′-UCU GCUUAAAGGUGAAAGUAGCAGG-3′;

BRCA2 siRNA (siBRCA2): 5′-GAAGAAUGCAGGUUUAAU-3′;

RFC1 siRNA (siRFC1): 5′-GAAGGCGGCCUCUAAAUCAUU-3′;

RAD17 siRNA (siRAD17): 5′-CAGACUGGUUGACCCAUCUU-3′;

PCNA siRNA (siPCNA): 5′-GGAGGAAGCUGUUACCAUAUU-3′;

MRE11 siRNA (siMRE11): Dharmacon SMARTpool M-009271-01-0005;

POLD3 siRNA (siPOLD3): #1, Invitrogen 4390824-s21045, #2, Invitrogen 4392420-s21046;

POLD1 siRNA (siPOLD1): #1, Invitrogen 4392420-s615, #2, Invitrogen 4392420-s616;

POLD4 siRNA (siPOLD4): 5′-GCAUCUCUAUCCCCUAUGAUU-3′;

POLE siRNA (siPOLE): #1, 5′-GGACAGGCGUUACGAGUUCUU-3′; #2, 5′-CU CGGAAGCUGGAAGAUUAUU-3′;

POLA1 siRNA (siPOLA1): #1, Invitrogen 4392420-s10772, #2, Invitrogen 4392420-s10774;

REV3L siRNA (siREV3L): 5′-CCCACUGGAAUUAAUGCACAAUU-3′;

PRIM1 siRNA (siPRIM1): Invitrogen HSS108448;

MCM2 siRNA (siMCM2): Invitrogen HSS106390;

MCM7 siRNA (siMCM7): Invitrogen HSS106405;

POLH siRNA (siPOLH): 5′-CTGGTTGTGAGCATTCGTGTA-3′;

REV1 siRNA (siREV1): 5′-ATCGGTGGAATCGGTTTGGAA-3′;

Knockdown efficiencies were evaluated by western blot (Extended Data Fig. 9). The following CRISPR sgRNA sequences were used:

sg*POLD3*: #1, 5′-GCAGATAAAGCTGGTCCGCCA-3′, #2, 5′-GAAATA TAGACGAGTTCGTCA-3′;

sg*HOP2*: #1, 5′-GCCGGACGTTGTAGTTGCTCG-3′, #2, 5′-GCGGGAAA GGCGATGAGTAA-3′, #3, 5′-GCGGGAGGTAACGGCGCCGT-3′, #4, 5′-GAGT AGATTCACCCGTTGTC-3′, #5, 5′-GACCCATGAGAGCCCGACAAC-3′.

Antibodies

The following antibodies were used: anti-BrdU (mouse B44, BD 347580; rat BU1/75, AbD Serotec OBT0030G), anti-ATRX (rabbit H-300, Santa Cruz sc-15408), anti-53BP1 (rabbit, Novus NB100-904), anti-γH2AX (mouse JBW301, Millipore 05-636), anti-Flag (mouse M2, Sigma F1804), anti-PML (mouse PG-M3, Santa Cruz sc-966), anti-Rad51 (rabbit H-92, Santa Cruz sc-8349; mouse 14B4, Abcam ab-213), anti-Hop2/PSMC3IP (rabbit, Novus NBP1-92301), anti-POLD3 (mouse 3E2, Abnova H00010714-M01), anti-POLD1 (mouse

607, Abcam ab10362; rabbit, Bethyl A304-005A), anti-POLD2 (rabbit, Bethyl A304-322A), anti-POLD4 (mouse 2B11, Abnova H00057804-M01A), anti-POLE (mouse 93H3A, Pierce MA5-13616; rabbit, Novus NBP1-68470), anti-POLE3 (rabbit, Bethyl A301-245A), anti-POLA1 (rabbit, Bethyl A302-851A), anti-MCM7 (rabbit, Bethyl A302-584A), anti-MCM4 (rabbit, Bethyl A300-193A), anti-MCM5 (rabbit, Abcam ab75975), anti-RFC1 (rabbit, Bethyl A300-320A), anti-PCNA (mouse PC10, CST #2586) anti-ATR (goat N-17, Santa Cruz sc-1887), anti-PRIM1 (rabbit H300, Santa Cruz sc-366482), anti-Rad17 (goat, Bethyl A300-151A), anti-REV3L (rabbit, GeneTex GTX100153), anti-POLH (rabbit, Bethyl A301-231A), anti-REV1 (rabbit H300, Santa Cruz sc-48806) anti-GAPDH (rabbit 14c10, CST #2118), anti-αTubulin (mouse TU-02, Santa Cruz sc-8035).

Drugs

Doxycycline was used at a concentration of 40 ng ml^{-1} for 16–24 h to induce expression of TRF1–FokI. Shield-1 (Cheminpharma LLC) and 4-hydroxytamoxifen (4-OHT) (Sigma-Aldrich) were both used at a concentration of 1 μM for 2 h, unless otherwise stated, in to allow for TRF1–FokI stabilization and translocation into the nucleus. RO-3306 (Selleck Chemicals) was used at a concentration of 10 μM for 20–24 h. G2 enrichment was confirmed by propidium iodide staining and flow cytometry. Colcemid (Roche) was used at a concentration of 100 ng ml^{-1}. The ATR inhibitor VE-821 (Selleck Chemicals) and Chk1 inhibitor LY2603618 (Selleck Chemicals) were used at a concentration of 5 μM and 1 μM respectively for 24 h.

Western blot

Cells were lysed in RIPA buffer supplemented with cOmplete protein inhibitor cocktail (Roche) and Halt phosphatase inhibitor cocktail (Thermo) on ice and subsequently spun down at max speed at 4 °C. The supernatant was removed and protein concentration determined using the Protein Assay Dye Reagent (Bio-Rad). 20–40 μg of protein was run on a 4–12% Bis–Tris gel (Invitrogen). Proteins were transferred onto an Amersham Protran 0.2 μm nitrocellulose membrane (GE) and blocked with 5% milk. Membranes were incubated with primary antibodies overnight at 4 °C. The next day membranes were incubated with secondary antibodies for 1 h at room temperature and subsequently developed using Western Lightning Plus-ECL (Perkins Elmer) or SuperSignal West Femto (Thermo).

Immunofluorescence, immunofluorescence–FISH, TIF assay, APB assay, and CO-FISH

Cells grown on coverslips were fixed in 4% paraformaldehyde for 10 min at room temperature. Coverslips were then permeabilized in 0.5% Triton X-100 for 5 min at 4 °C (for most antibodies) or 100% cold methanol for 10 min at −20 °C (for anti-PCNA). Primary antibody incubation was performed at 4 °C in a humidified chamber overnight unless otherwise indicated. Coverslips were washed and incubated with appropriate secondary antibody for 20 min at 37 °C, then mounted onto glass slides using Vectashield mounting medium with DAPI (Vector Labs). For immunofluorescence–FISH, coverslips were re-fixed in 4% paraformaldehyde for 10 min at room temperature after secondary antibody binding. Coverslips were then dehydrated in an ethanol series (70%, 90%, 100%) and allowed to air dry. Dehydrated coverslips were denatured and incubated with TelC–Cy3 peptide nucleic acid (PNA) probe (Panagene) in hybridization buffer (70% deionized formamide, 10 mM

Tris (pH 7.4), 0.5% Roche blocking solution) overnight at room temperature in a humidified chamber. The next day, coverslips were washed and mounted as described above. Images were acquired with a QImaging RETIGA-SRV camera connected to a Nikon Eclipse 80i microscope. For TIF assay, cells were scored for co-localized 53BP1 and telomere foci by immunofluorescence–FISH. For APB assay, cells were scored for the number of PML–telomere colocalizations by immunofluorescence–FISH. Hop2 immunofluorescence and CO–FISH experiments were performed as previously described[7].

Pulsed-field gel electrophoresis and in-gel hybridization

Telomere gels were performed using telomere restriction fragment (TRF) analysis. Genomic DNA was digested using AluI and MboI (NEB). 4–10 μg of DNA was run on a 1% PFGE agarose gel (Bio-Rad) in 0.5× TBE buffer using the CHEF-DRII system (Bio-Rad) at 6 V cm^{-1}; initial switch time 5 s, final switch time 5 s, for 16 h at 14 °C. The gel was then dried for 4 h at 50 °C, denatured in a 0.5 N NaOH 1.5 M NaCl solution, and neutralized. Gel was hybridized with ^{32}P-labelled $(CCCTAA)_6$ oligonucleotides in Church buffer overnight at 42 °C. The next day, the membrane was washed four times in 4× SSC buffer, exposed onto a storage phosphor screen (GE Healthcare) and scanned using STORM 860 with ImageQuant (Molecular Dynamics). Telomere length was determined using TeloTool software[35].

C-circle assay

C-circle assay was performed as previously described[28]. Genomic DNA was digested using AluI and MboI (NEB). 30 ng of digested DNA was combined with 0.2 mg ml^{-1} BSA, 0.1% Tween, 1 mM each dNTP without dCTP, 1× φ29 Buffer (NEB) and 7.5 U ϕ29 DNA polymerase (NEB). Samples were incubated for 8 h at 30 °C followed by 20 min at 65 °C. Samples were then diluted in 2× SSC buffer and dot-blotted onto an Amersham Hybond-N^+ nylon membrane (GE). Membrane was ultraviolet crosslinked and then hybridized with ^{32}P-labelled $(CCCTAA)_6$ oligonucleotides in PerfectHyb Plus Hybridization Buffer (Sigma) overnight at 37 °C. The next day, the membrane was washed twice in 2× SSC buffer, exposed onto a storage phosphor screen (GE Healthcare) and scanned using STORM 860 with ImageQuant (Molecular Dynamics).

Co–immunoprecition and chromatin immunoprecipitation (ChIP)

Cells were lysed in HEPES immunoprecipitation buffer (10 mM HEPES (pH 8), 2 mM EDTA, 0.1% NP-40) supplemented with 5 mM DTT, 1 mM PMSF, and 1× cOmplete protein inhibitor cocktail (Roche) on ice and subsequently spun down at max speed at 4 °C. The supernatant was removed and protein concentration determined using the Protein Assay Dye Reagent (Bio-Rad). 25 μg protein was removed for input. 500 μg protein was diluted to 1 mg ml^{-1} in HEPES immunoprecipitation buffer and pre-cleared with 10 μl Protein G magnetic beads (Pierce) for 1 h rotating at 4 °C. Protein lysate was then incubated with 10 μg anti-IgG (Sigma) or anti-POLD1 antibody (Abcam) rotating overnight at 4 °C. The next day, samples were incubated with 30 μl Protein G magnetic beads (Pierce) that had been pre-bound to a bridging antibody (Active Motif) for 1 h rotating at 4 °C. Beads were subsequently washed five times with HEPES immunoprecipiation buffer. Proteins were eluted by incubating beads with 2× sample buffer with BME for 5 min at 95 °C. Samples were analysed by western

blot. ChIP was performed as previously described and analysed by western blot and dot blot[36].

Telomere content dot blot

400 ng of genomic DNA was diluted into 2× SSC buffer, treated at 95 °C for 5 min, and dot-blotted onto an Amersham Hybond-N^+ nylon membrane (GE). Membrane was then denatured in a 0.5 N NaOH 1.5 M NaCl solution, neutralized, and UV crosslinked. Membrane was hybridized with ^{32}P-labelled $(CCCTAA)_6$, or Alu repeat oligonucleotides in PerfectHyb Plus Hybridization Buffer (Sigma) overnight at 37 °C. The next day, the membrane was washed twice in 2× SSC, exposed onto a storage phosphor screen (GE Healthcare) and scanned using STORM 860 with ImageQuant (Molecular Dynamics).

Live cell imaging and image analysis

Live cell imaging was performed and analysed as previously described[7]. Fixed cell and live cell images were captured at 60× and 100× magnification, respectively. Microscope images and dot blots were prepared and analysed using Fiji. Southern blot telomere gel images were prepared using Fiji and were not cropped to exclude any part of the presented lanes. Western blot gel images were prepared using Adobe Photoshop and cropped to present relevant bands. Uncropped western blot images are shown in Supplementary Fig. 1.

Statistics

All statistical analysis was done using GraphPad Prism 5 software. Unpaired *t*-tests were used to generate two-tailed *P* values.

Extended Data

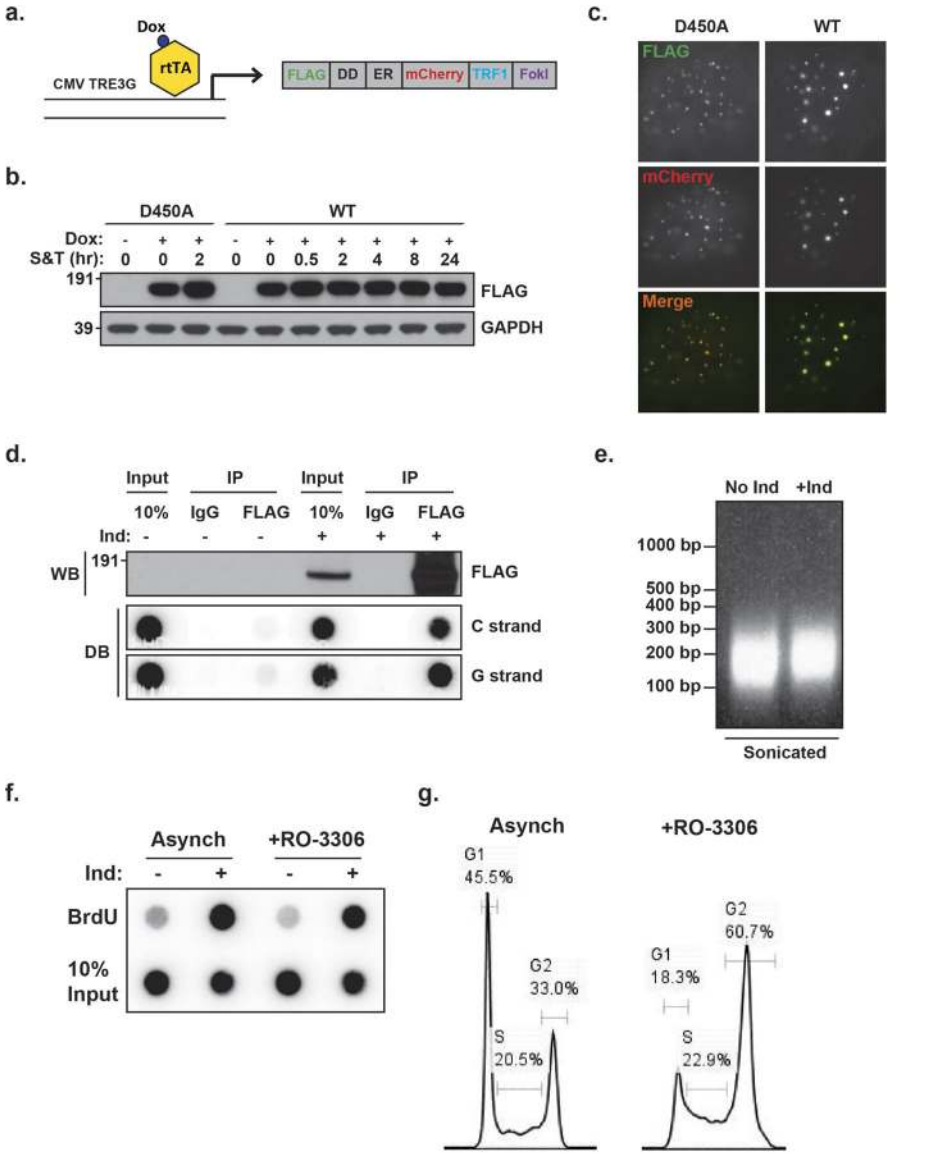

Extended Data Figure 1. An inducible system for studying break-induced telomere synthesis

a, Schematic of inducible TRF1–FokI system. **b**–**d**, Characterization of U2OS inducible TRF1–FokI system by western blot (**b**), immunofluorescence (**c**), and telomere ChIP (**d**). **e**, Agarose gel of sonicated DNA prepared for BrdU pulldown. **f**, **g**, BrdU pulldown dot blot for telomere content (**f**) from asynchronous or G2-enriched U2OS cells induced (Ind) with TRF1–FokI for 2 h, with cell-cycle profiles by propidium iodide staining (**g**). Images were captured at 60× magnification. Dox, doxycycline; S, Shield-1; *T*, 4-hydroxytamoxifen; DD, destabilization domain; ER, oestrogen receptor; rtTA, reverse tetracycline transactivator; TRE3G, tetracycline response element; WT, wild-type; D450A, nuclease-null mutant.

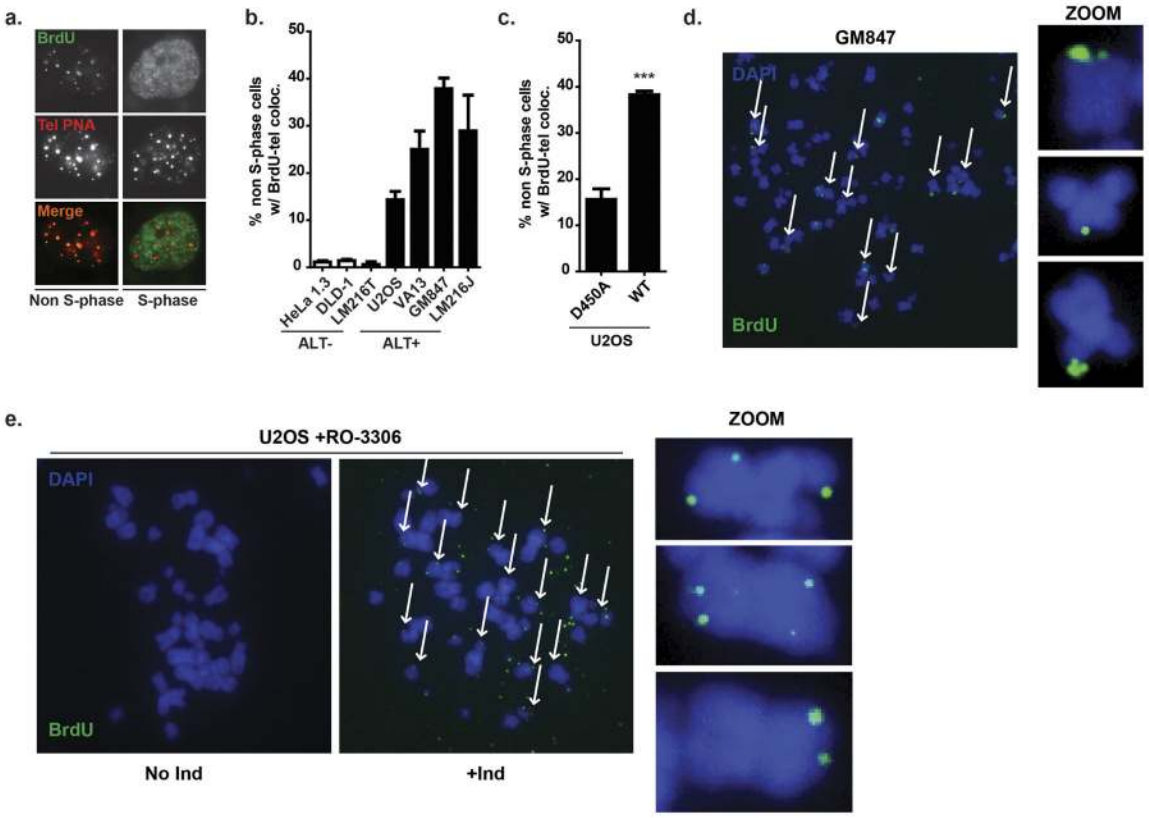

Extended Data Figure 2. Visualization of spontaneous ALT telomere synthesis

a–**c**, BrdU immunofluorescence assay to visualize spontaneous ALT telomere synthesis, with representative images of VA13 cells (**a**) and quantification of a panel of ALT^{-} and ALT^{+} cell lines (**b**) and U2OS cells induced with TRF1–FokI for 2 h (**c**). **d**, **e**, Representative images of BrdU immunofluorescence of metaphases from spontaneous GM847 cells (**d**) and U2OS induced (+Ind) with TRF1–FokI for 2 h upon release from RO-3306 (**e**). Images were captured at 60× magnification. Data represent mean ± s.e.m. of three independent experiments. ***$P \leq 0.001$.

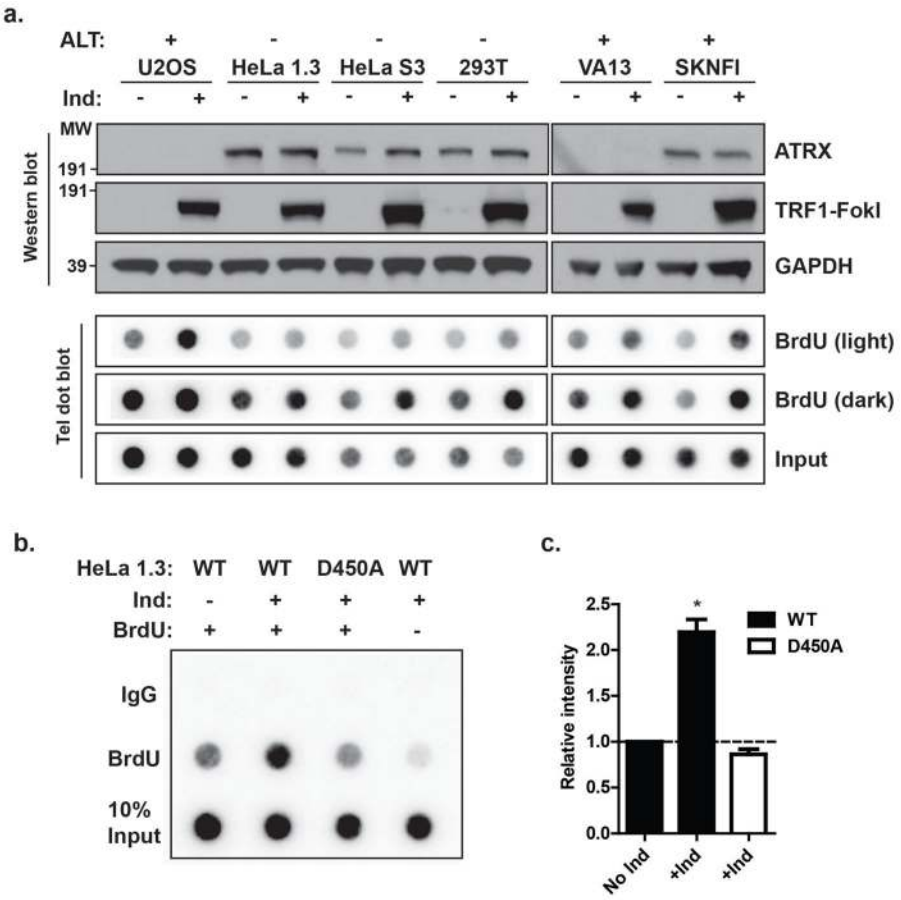

Extended Data Figure 3. Break-induced telomere synthesis occurs independently of telomere maintenance mechanism

a, A panel of ALT^{-} and ALT^{+} inducible TRF1–FokI cell lines tested for TRF1–FokI and ATRX expression by western blot and nascent telomere synthesis by BrdU pulldown dot blot for telomere content after induction (Ind) with TRF1–FokI for 2 h. **b**, **c**, BrdU pulldown dot blot for telomere content (**b**) from HeLa 1.3 cells induced (Ind) with TRF1–FokI for 2 h, with quantification (**c**). Data represent mean ± s.e.m. of two independent experiments. *$P \leq 0.05$.

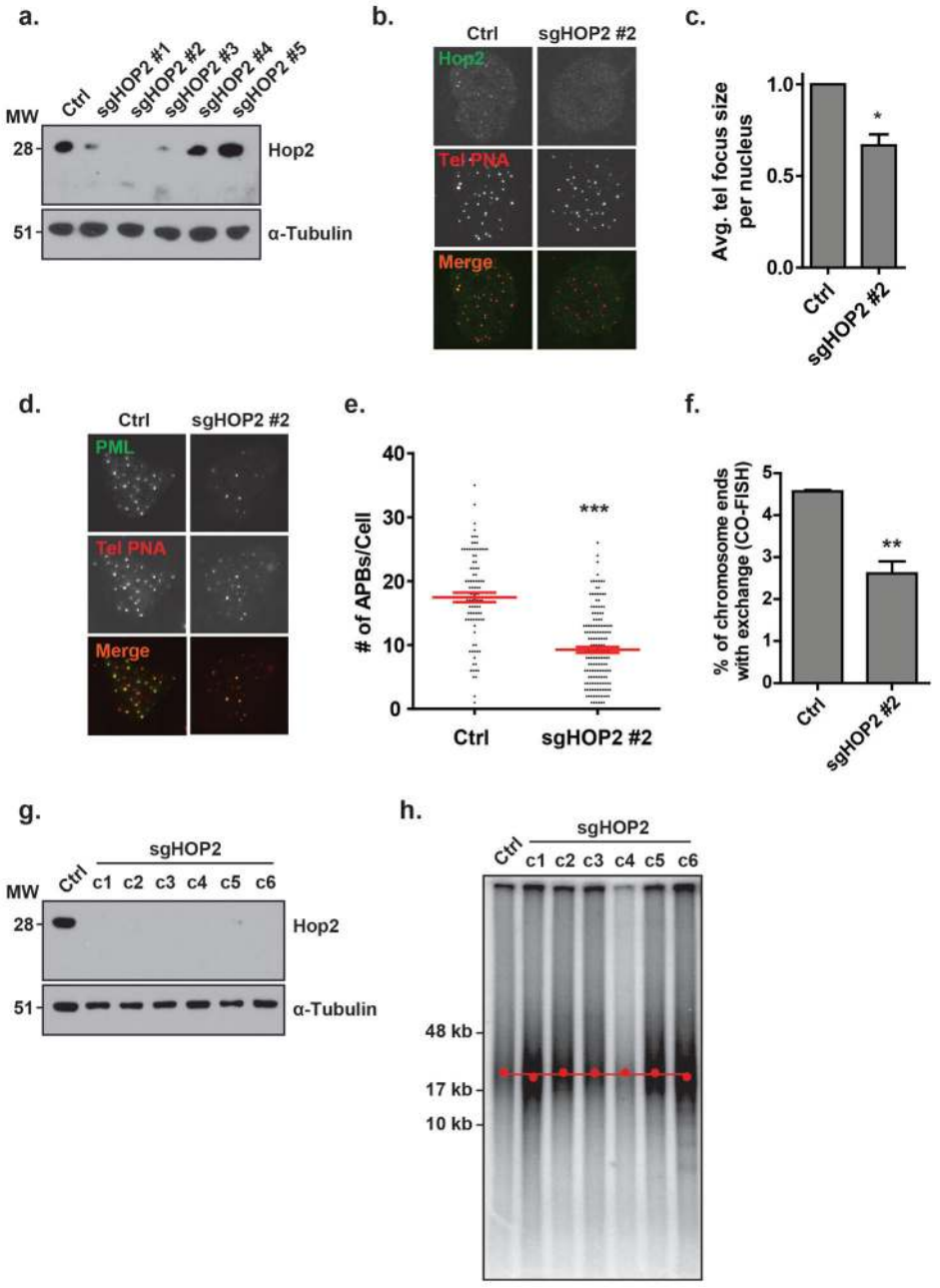

Extended Data Figure 4. Hop2 contributes to telomere clustering but is dispensable for telomere length maintenance

a–h, CRISPR/Cas9-mediated excision of *HOP2* (sg*HOP2*) in VA13 cells, with western blot of populations (**a**). Analysis of Hop2 co-localization with telomere foci by IF-FISH (**b**), telomere focus size by FISH (**c**), APBs by PML co-localization with telomere foci (**d**, **e**), and telomere exchanges by CO-FISH (**f**) from sg*HOP2* #2 population. Analysis of clones (c1–c6) by western blot (**g**) and TRF pulsed-field gel at ~PD 25 (**h**). Peak intensity of telomere length is indicated by red dot. Images were captured at 60× magnification. Data represent mean ± s.e.m. of at least two independent experiments. ***P <0.0005, **P <0.005, *P <0.05.

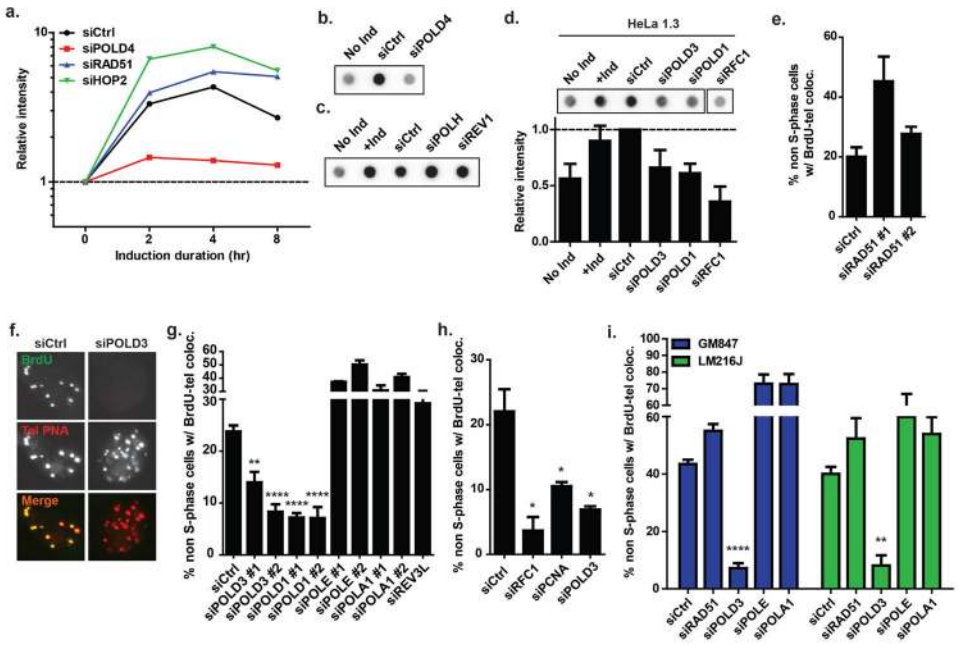

Extended Data Figure 5. Requirements for break-induced and spontaneous ALT telomere synthesis

a, BrdU pulldown dot blot timecourse for telomere content from U2OS induced (Ind) with TRF1-FokI for indicated times and treated with indicated siRNAs. **b**, **c**, BrdU pulldown dot blots for telomere content from U2OS induced (Ind) with TRF1–FokI for 2 h and treated with indicated siRNAs. **d**, BrdU pulldown dot blot for telomere content from HeLa 1.3 induced (Ind) with TRF1–FokI for 2 h and treated with indicated siRNAs, with quantification. **e**–**i**, Analysis of spontaneous ALT telomere synthesis using BrdU immunofluorescence from VA13 (**e**–**h**) and GM847 and LM216J (**i**) treated with indicated siRNAs. Images were captured at 60× magnification. Data represent mean ± s.e.m. of two (**d**) or three (**e**–**i**) independent experiments. ****$P \leq 0.0001$, **$P \leq 0.01$, *$P \leq 0.05$.

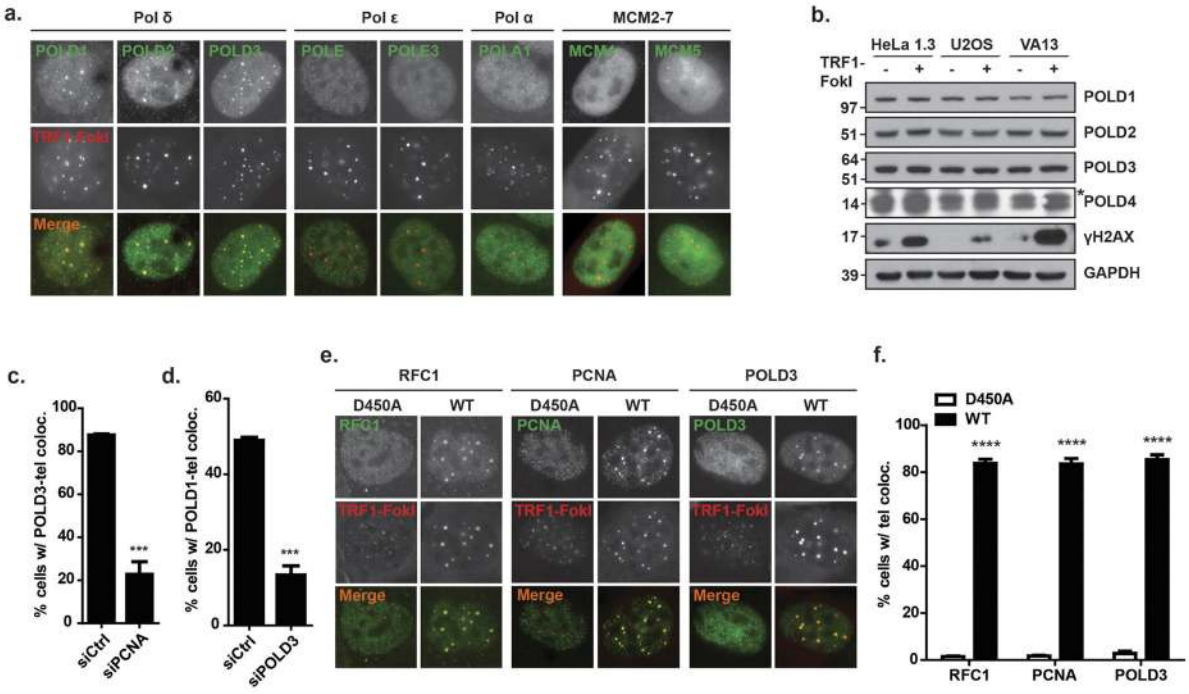

Extended Data Figure 6. Pol δ predominates at ALT telomeres

a, Representative images of replisome components (green) and telomere foci (red) from U2OS induced with TRF1–FokI for 2 h. **b**, western blot of Pol δ complex from cell lines treated with TRF1–FokI. Asterisk denotes non-specific band. **c**, **d**, Quantification of co-localized POLD3 (**c**) or POLD1 (**d**) with telomere foci from U2OS induced with TRF1–FokI for 2 h. **e**, **f**, Representative images (**e**) of co-localized RFC1-PCNA-POLD3 (green) and telomere foci (red) from U2OS induced with TRF1–FokI for 2 h, with quantification (**f**). WT =wild-type, D450A =nuclease-null mutant. Images were captured at 60× magnification. Data represent mean ± s.e.m. of three independent experiments. ****$P \leq 0.0001$, ***$P \leq 0.001$.

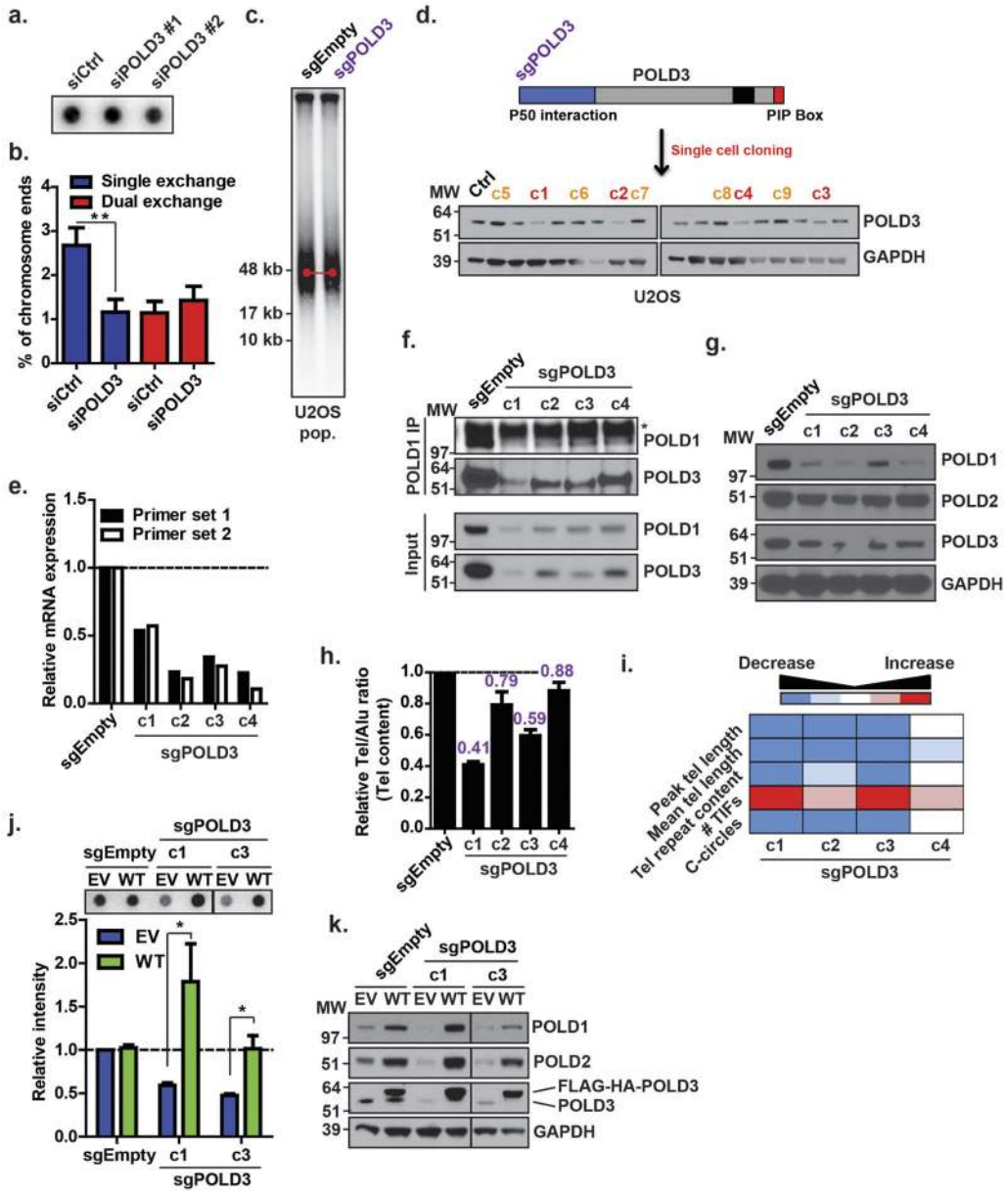

Extended Data Figure 7. POLD3 is critical for telomere maintenance in ALT-dependent cells

a, **b**, analysis of transient POLD3 depletion by C-circle dot blot (**a**) from U2OS and CO-FISH (**b**) from VA13 (n =1780 ends for siCtrl, n = 1637 ends for siPOLD3). **c**, TRF analysis from U2OS populations at ~PD 25. Peak intensity of telomere length is indicated by red dot. **d**, schematic of U2OS POLD3 CRISPR (sg*POLD3*) cloning strategy with western blot. **e**–**g**, analysis of POLD3 expression from U2OS clones c1–c4 by qPCR (**e**), POLD1 Co–IP (**f**), and darker exposure of western blot from Fig. 4a (**g**). Asterisk denotes non-specific band. **h**, Quantification of relative telomere content by dot blot from U2OS clones c1–c4. **i**, Heat map summarizing decreases (blue), increases (red), or no change (white) in telomere maintenance from U2OS clones c1–c4 as compared to U2OS control. **j**, **k**, POLD3-reconstituted CRISPR clones analysed for C-circles by dot blot (**j**) and Pol δ expression by western blot (**k**). EV,

empty vector; WT, reconstituted POLD3. Data represent mean ± s.e.m. of two independent experiments. $^{**}P \leq 0.01$, $^{*}P \leq 0.05$.

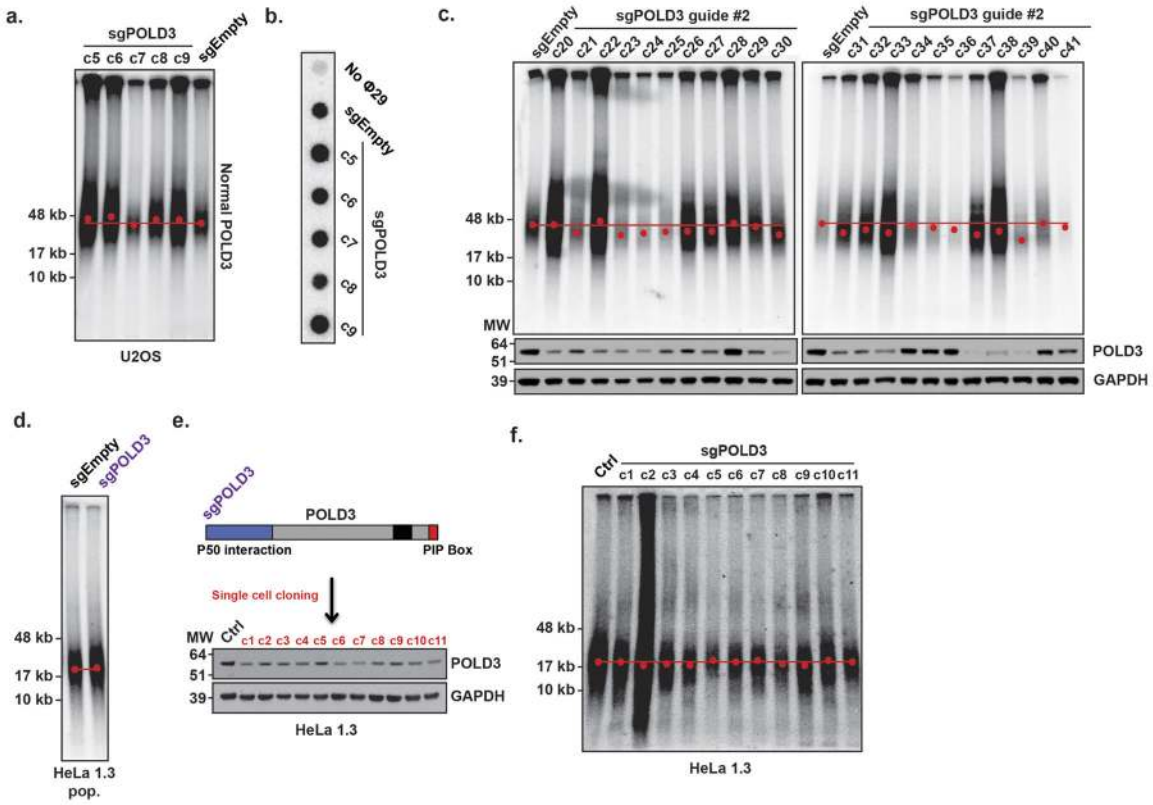

Extended Data Figure 8. Extended analysis of POLD3 CRISPR clones

a, **b**, TRF analysis by pulsed-field gel (**a**) and C-circle dot blot (**b**) from U2OS POLD3 CRISPR (sg*POLD3*) clones with normal POLD3 expression (c5–c9) at ~PD 25. **c**, U2OS POLD3 CRISPR clones from an independent guide RNA (sg*POLD3* #2) analysed by TRF and western blot at ~PD 25. **d**, TRF analysis by pulsed-field gel from HeLa 1.3 populations at ~PD 25. **e**, Schematic of HeLa 1.3 POLD3 CRISPR cloning strategy with western blot. **f**, TRF analysis by pulsed-field gel from HeLa 1.3 clones c1–c11 at ~PD 25. Peak intensity of telomere length is indicated by red dot.

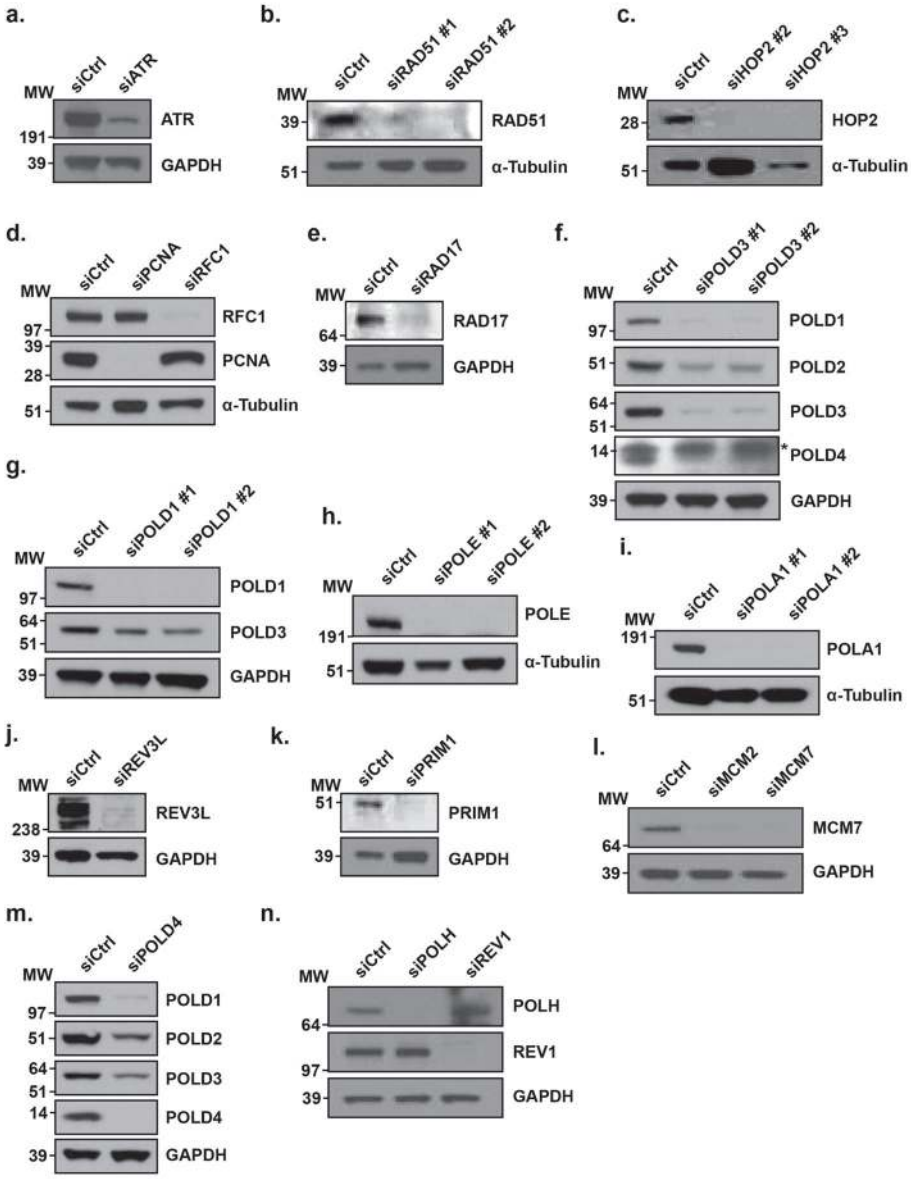

Extended Data Figure 9. Knockdown efficiencies

a–n, Western blots of U2OS or VA13 cells treated with indicated siRNAs. Asterisk denotes non-specific band.

Supplementary Material

Refer to Web version on PubMed Central for supplementary material.

Acknowledgments

We thank A. Sfeir and A. Phillips (NYU) for guidance on telomere SMARD experiments and members of the Greenberg laboratory for critical discussion. This work was supported by NIH grants GM101149, CA138835, and CA17494 to R.A.G., who is also supported by funds from the Abramson Family Cancer Research Institute and Basser Research Center for BRCA. R.L.D. was supported by NIH grants T32GM007170 and T32GM008216.

References

1. Ciccia A, Elledge SJ. The DNA damage response: making it safe to play with knives. Mol Cell. 2010; 40:179–204. [PubMed: 20965415]
2. Bryan TM, Englezou A, Gupta J, Bacchetti S, Reddel RR. Telomere elongation in immortal human cells without detectable telomerase activity. EMBO J. 1995; 14:4240–4248. [PubMed: 7556065]
3. Cesare AJ, Reddel RR. Alternative lengthening of telomeres: models, mechanisms and implications. Nat Rev Genet. 2010; 11:319–330. [PubMed: 20351727]
4. Norio P, Schildkraut C. Visualization of DNA replication on individual Epstein-Barr virus episomes. Science. 2001; 294:2361–2365. [PubMed: 11743204]
5. Sfeir A, et al. Mammalian telomeres resemble fragile sites and require TRF1 for efficient replication. Cell. 2009; 138:90–103. [PubMed: 19596237]
6. Nabetani A, Yokoyama O, Ishikawa F. Localization of hRad9, hHus1, hRad1, and hRad17 and caffeine-sensitive DNA replication at the alternative lengthening of telomeres-associated promyelocytic leukemia body. J Biol Chem. 2004; 279:25849–25857. [PubMed: 15075340]
7. Cho NW, Dilley RL, Lampson MA, Greenberg RA. Interchromosomal homology searches drive directional ALT telomere movement and synapsis. Cell. 2014; 159:108–121. [PubMed: 25259924]
8. O'Sullivan RJ, et al. Rapid induction of alternative lengthening of telomeres by depletion of the histone chaperone ASF1. Nat Struct Mol Biol. 2014; 21:167–174. [PubMed: 24413054]
9. Lundblad V, Blackburn EH. An alternative pathway for yeast telomere maintenance rescues est1- senescence. Cell. 1993; 73:347–360. [PubMed: 8477448]
10. Teng SC, Zakian VA. Telomere-telomere recombination is an efficient bypass pathway for telomere maintenance in *Saccharomyces cerevisiae*. Mol Cell Biol. 1999; 19:8083–8093. [PubMed: 10567534]
11. Le S, Moore JK, Haber JE, Greider CW. *RAD50* and *RAD51* define two pathways that collaborate to maintain telomeres in the absence of telomerase. Genetics. 1999; 152:143–152. [PubMed: 10224249]
12. Lydeard JR, Jain S, Yamaguchi M, Haber JE. Break-induced replication and telomerase-independent telomere maintenance require Pol32. Nature. 2007; 448:820–823. [PubMed: 17671506]
13. Malkova A, Ivanov EL, Haber JE. Double-strand break repair in the absence of *RAD51* in yeast: a possible role for break-induced DNA replication. Proc Natl Acad Sci USA. 1996; 93:7131–7136. [PubMed: 8692957]
14. Chen Q, Ijpma A, Greider CW. Two survivor pathways that allow growth in the absence of telomerase are generated by distinct telomere recombination events. Mol Cell Biol. 2001; 21:1819–1827. [PubMed: 11238918]
15. Teng SC, Chang J, McCowan B, Zakian VA. Telomerase-independent lengthening of yeast telomeres occurs by an abrupt Rad50p-dependent, Rif-inhibited recombinational process. Mol Cell. 2000; 6:947–952. [PubMed: 11090632]
16. Cox KE, Maréchal A, Flynn RL. SMARCAL1 resolves replication stress at ALT telomeres. Cell Reports. 2016; 14:1032–1040. [PubMed: 26832416]
17. Yeager TR, et al. Telomerase-negative immortalized human cells contain a novel type of promyelocytic leukaemia (PML) body. Cancer Res. 1999; 59:4175–4179. [PubMed: 10485449]
18. Flynn RL, et al. Alternative lengthening of telomeres renders cancer cells hypersensitive to ATR inhibitors. Science. 2015; 347:273–277. [PubMed: 25593184]
19. Lydeard JR, et al. Break-induced replication requires all essential DNA replication factors except those specific for pre-RC assembly. Genes Dev. 2010; 24:1133–1144. [PubMed: 20516198]
20. Johnson RE, Prakash L, Prakash S. Pol31 and Pol32 subunits of yeast DNA polymerase δ are also essential subunits of DNA polymerase ζ. Proc Natl Acad Sci USA. 2012; 109:12455–12460. [PubMed: 22711820]
21. Baranovskiy AG, et al. DNA polymerase δ and ζ switch by sharing accessory subunits of DNA polymerase δ. J Biol Chem. 2012; 287:17281–17287. [PubMed: 22465957]

22. Makarova AV, Stodola JL, Burgers PM. A four-subunit DNA polymerase ζ complex containing Pol δ accessory subunits is essential for PCNA-mediated mutagenesis. Nucleic Acids Res. 2012; 40:11618–11626. [PubMed: 23066099]
23. Ducoux M, et al. Mediation of proliferating cell nuclear antigen (PCNA)-dependent DNA replication through a conserved $p21^{Cip1}$-like PCNA-binding motif present in the third subunit of human DNA polymerase δ. J Biol Chem. 2001; 276:49258–49266. [PubMed: 11595739]
24. Chilkova O, et al. The eukaryotic leading and lagging strand DNA polymerases are loaded onto primer-ends via separate mechanisms but have comparable processivity in the presence of PCNA. Nucleic Acids Res. 2007; 35:6588–6597. [PubMed: 17905813]
25. Karras GI, Jentsch S. The *RAD6* DNA damage tolerance pathway operates uncoupled from the replication fork and is functional beyond S phase. Cell. 2010; 141:255–267. [PubMed: 20403322]
26. Murga M, et al. POLD3 is haploinsufficient for DNA replication in mice. Mol Cell. 2016; 63:877–883. [PubMed: 27524497]
27. Zhong ZH, et al. Disruption of telomere maintenance by depletion of the MRE11/RAD50/NBS1 complex in cells that use alternative lengthening of telomeres. J Biol Chem. 2007; 282:29314–29322. [PubMed: 17693401]
28. Henson JD, et al. DNA C-circles are specific and quantifiable markers of alternative-lengthening-of-telomeres activity. Nat Biotechnol. 2009; 27:1181–1185. [PubMed: 19935656]
29. Costantino L, et al. Break-induced replication repair of damaged forks induces genomic duplications in human cells. Science. 2014; 343:88–91. [PubMed: 24310611]
30. Mayle R, et al. Mus81 and converging forks limit the mutagenicity of replication fork breakage. Science. 2015; 349:742–747. [PubMed: 26273056]
31. Minocherhomji S, et al. Replication stress activates DNA repair synthesis in mitosis. Nature. 2015; 528:286–290. [PubMed: 26633632]
32. Miyabe I, et al. Polymerase δ replicates both strands after homologous recombination-dependent fork restart. Nat Struct Mol Biol. 2015; 22:932–938. [PubMed: 26436826]
33. Verma P, Greenberg RA. Noncanonical views of homology-directed DNA repair. Genes Dev. 2016; 30:1138–1154. [PubMed: 27222516]
34. Viggiani CJ, Knott SRV, Aparicio OM. Genome-wide analysis of DNA synthesis by BrdU immunoprecipitation on tiling microarrays (BrdU-IP-chip) in *Saccharomyces cerevisiae*. Cold Spring Harb Protoc. 2010 pdb.prot5385 (2010).
35. Göhring J, Fulcher N, Jacak J, Riha K. TeloTool: a new tool for telomere length measurement from terminal restriction fragment analysis with improved probe intensity correction. Nucleic Acids Res. 2014; 42:e21. [PubMed: 24366880]
36. Tang J, et al. Acetylation limits 53BP1 association with damaged chromatin to promote homologous recombination. Nat Struct Mol Biol. 2013; 20:317–325. [PubMed: 23377543]

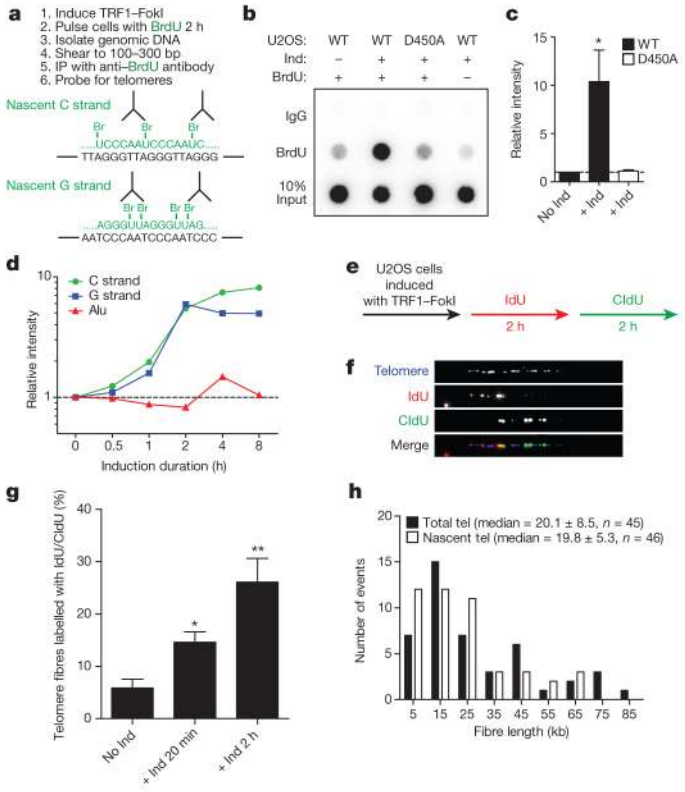

Figure 1. Break-induced telomere synthesis occurs by long-tract unidirectional telomeric recombination

a, Schematic of BrdU pulldown. IP, immunoprecipitation. **b–d**, BrdU pulldown dot blot for telomere content using a ^{32}P-labelled telomere oligonucleotide (**b**) from U2OS cells induced (Ind) with TRF1–FokI for 2 h, with quantification (**c**) and time course of C- and G-rich telomere strands compared to Alu repeats (**d**). **e**, Schematic of telomere SMARD. **f–h**, Representative images (**f**) of telomere (blue) labelled with IdU (red) and CldU (green) from U2OS cells induced (Ind) with TRF1–FokI, with quantification (**g**) and length of telomere fibres (**h**). Median length quantified ± 95% C.I. WT, wild-type; D450A, nuclease-null mutant. Data represent mean ± s.e.m. of three (**c**) or two (**g**) independent experiments. $^{**}P \leq 0.01$, $^{*}P \leq 0.05$.

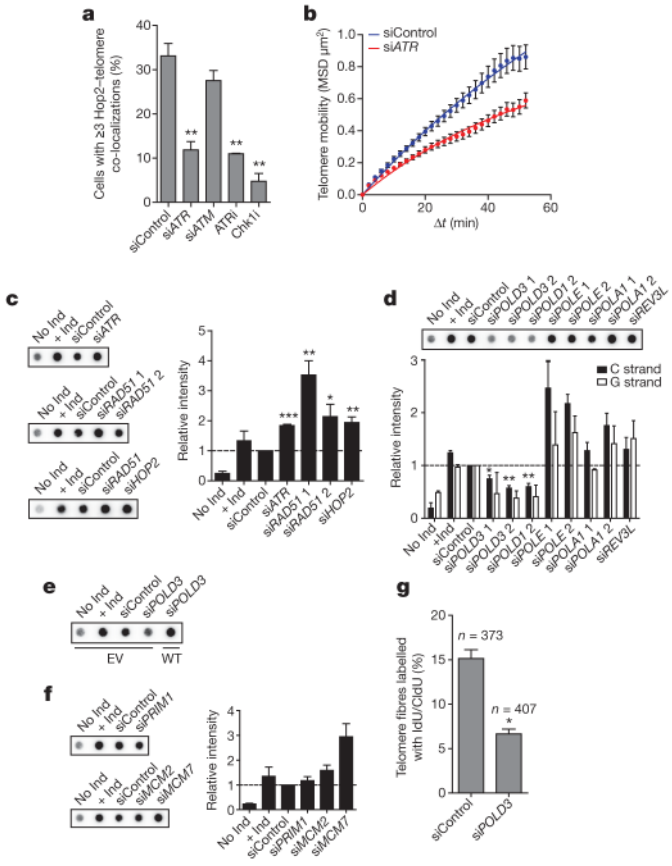

Figure 2. Break-induced telomere synthesis occurs by alternative HDR and utilizes a non-canonical replisome defined by Pol δ

a, Quantification of co-localized Hop2 and telomere foci in TRF1–FokI expressing VA13 cells treated with the indicated small interfering RNAs (siRNAs) or inhibitors. **b**, Mean squared displacement (MSD) analysis of live-cell telomere movement from U2OS cells following TRF1–FokI induction. **c–f**, BrdU pulldown dot blots for telomere content (**c**, **d**, **e**, **f**) from U2OS cells induced (Ind) with TRF1–FokI for 2 h, with rescue experiment (**e**), and quantifications (**c**, **d**, **f**). **g**, Quantification of telomere SMARD from U2OS cells induced with TRF1–FokI and treated with the indicated siRNAs. EV, empty vector; WT, reconstituted POLD3. Data represent mean ± s.e.m. of at least two independent experiments. ***$P \leq 0.001$, **$P \leq 0.01$, *$P \leq 0.05$.

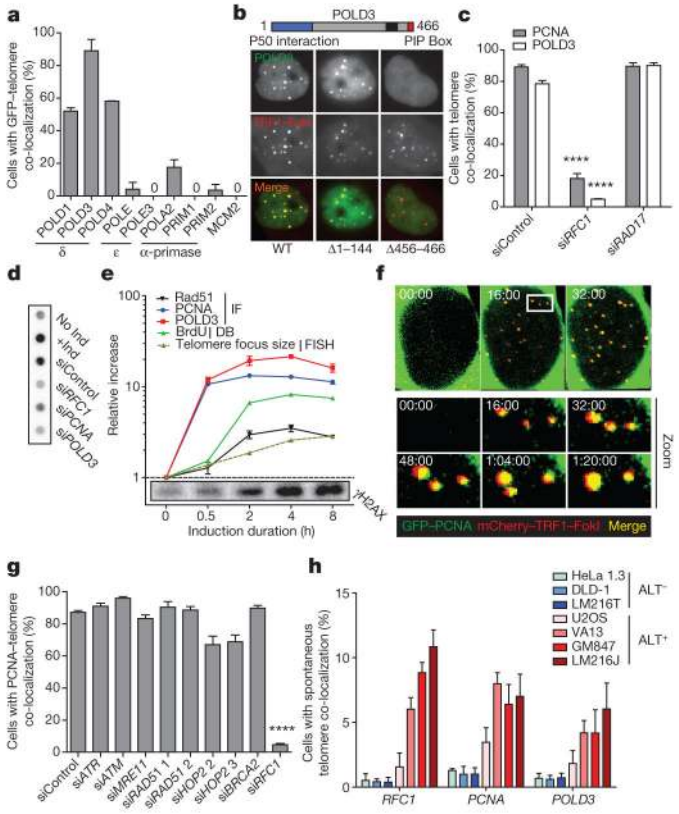

Figure 3. Rapid loading of PCNA acts as the initial sensor of telomere damage

a, Quantification of co-localized GFP-tagged replisome subunits and telomere foci from U2OS cells induced with TRF1–FokI for 2 h. **b**, Schematic of POLD3 and representative images of POLD3 deletion mutants. **c**, Quantification of co-localized endogenous PCNA and POLD3 and telomere foci from U2OS cells induced with TRF1–FokI for 2 h. **d**, BrdU pulldown dot blot for telomere content from U2OS cells induced (Ind) with TRF1–FokI for 2 h. **e**, Kinetics of PCNA and POLD3 loading at damaged telomeres in relation to Rad51, γH2AX, and DNA synthesis in U2OS cells. IF, immunofluorescence. **f**, Representative live-cell imaging of PCNA recruitment to damaged telomeres before telomere clustering in U2OS cells. Time in minutes shown in upper left corners. **g**, Quantification of the requirements for PCNA loading at damaged telomeres in U2OS cells. **h**, Quantification of spontaneous co-localized RFC1, PCNA, and POLD3 and telomere foci from a panel of ALT^{-} and ALT^{+} cell lines. Fixed cell and live cell images were captured at 60× and 100× magnification, respectively. Data represent mean ± s.e.m. of two (**a**) or three (**c**, **e**, **g**, **h**) independent experiments. ****$P \leq 0.0001$.

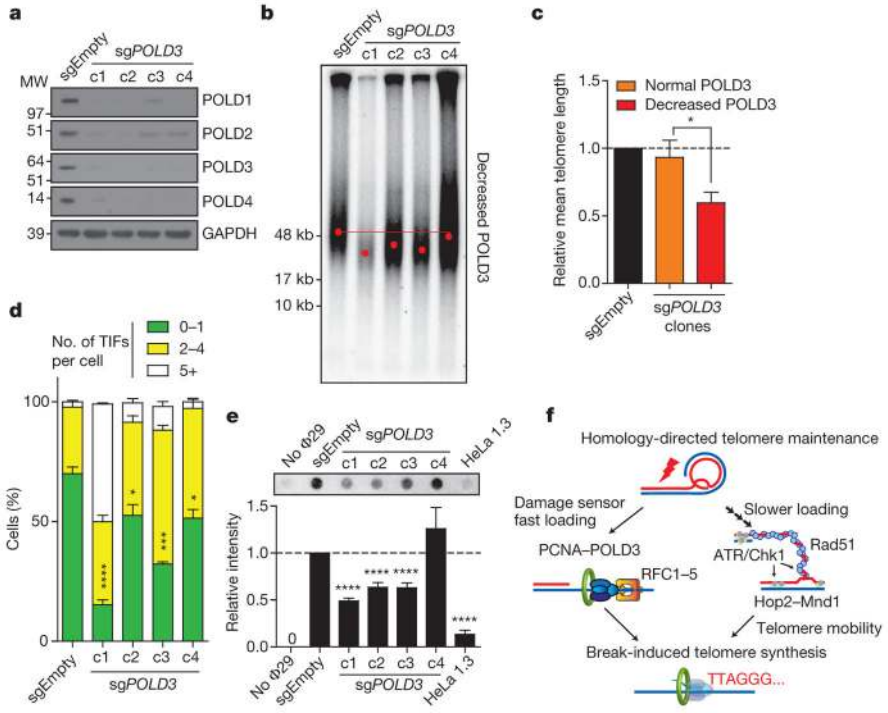

Figure 4. POLD3 is critical for telomere maintenance in ALT-dependent cells

a, Analysis of Pol δ protein expression by western blot from U2OS CRISPR clones (sg*POLD3*) with decreased POLD3 expression (c1–c4) compared to empty guide control (sgEmpty). GAPDH is used as a loading control. Darker exposure shown in Extended Data Fig. 7g. **b**, TRF analysis using pulsed-field gel electrophoresis from U2OS clones c1–c4 at ~PD 25. Peak intensity of telomere length is indicated by red dot. **c**, Quantification of relative mean telomere length in 31 pooled sg *POLD3* clones from two independent guide RNAs with normal and decreased POLD3 protein expression. **d**, **e**, Analysis of telomere maintenance by TIF quantification (co-localized 53BP1 and telomere foci) (**d**) and C-circle assay (**e**) from U2OS clones c1–c4. **f**, Model. Data represent mean ±s.e.m. of three independent experiments. ****$P \leq 0.0001$, ***$P \leq 0.001$, *$P \leq 0.05$.